CV chondrites: More than one parent body

J. Gattacceca, L. Bonal, C. Sonzogni, J. Longerey

CV chondrites: more than one parent body

J. Gattacceca[1], L. Bonal[2], C. Sonzogni[1], J. Longerey[1].

[1] CNRS, Aix Marseille Univ, IRD, Coll France, INRAE, CEREGE, Aix-en-Provence, France

[2]Institut de Planétologie et d'Astrophysique de Grenoble, Université Grenoble Alpes, CNRS CNES, 38000 Grenoble, France

Corresponding author: gattacceca@cerege.fr

Abstract

CV chondrites are one of the most studied group of carbonaceous chondrites. Based on a number of mineralogical features, they have been divided into three sub-groups: CV_{OxA}, CV_{OxB}, and CV_{Red}. These sub-groups are classically interpreted as coming from a single parent body, with a common protolith affected by significant parent body fluid-assisted metasomatism occurring at different temperatures and/or redox conditions. In this work, we studied a set of 53 CV chondrites. We classified them into the three sub-groups, measured their apparent chondrule sizes and their matrix modal abundance. We measured the triple oxygen isotopic composition for 17 of them. The distributions of chondrule size and matrix abundances in CV_{OxA} and CV_{OxB} cannot be statistically distinguished. Conversely, CV_{Red} and CV_{Ox} have distinct distributions. These two robust and simple petrographic indicators combined with the previous knowledge of the peak metamorphic temperatures experienced by these meteorites show that CV_{Ox} and CV_{Red} originate from two distinct parent bodies. On the other hand, CV_{OxA} and CV_{OxB} likely originate from the same parent body, with CV_{OxA} representing deeper, more metamorphosed levels. For clarification of the chondrite

classification scheme, in which one group should ultimately represent a single parent body, we propose to divide the CV group into two proper groups (and not subgroups as is the current scheme), keeping the names CV_{Red} and CV_{Ox}. These two groups can be readily separated by estimating the average nickel content of their sulfides.

1. Introduction

Most meteorites come from the main asteroid belt. They are extracted from asteroids by impact under the form of meteoroids (~ centimeter- to meter-sized objects), that orbit in the interplanetary space for typically a few Myr before colliding with the Earth (e.g., Eugster et al., 2006; Gravnik and Brown, 2018). The 60000 meteorites registered to date by the Meteoritical Society are classified into groups (e.g., Weisberg et al., 2006). The general idea behind grouping is that meteorites from a group derive from the same primary parent body (*senso* Greenwood et al. (2020), i.e., the source body from which the meteorite ultimately derived), in most cases an asteroid. This is strictly applicable to chondrites, the classification for achondrites being a little less coherent. For instance, meteorites originating from asteroid Vesta are separated into three groups (eucrites, diogenites, howardites) and meteorites originating from Mars are separated into several groups as well (shergottites, nakhlites, …). However, even for chondrites, it is not established that all meteorites within a group come from a single parent body, although this would be the ultimate objective of the classification scheme. CM chondrites, for instance, have been proposed to come from multiple parent bodies (e.g., Lee et al. 2019), but there has been no success in separating them into coherent sub-groups originating from distinct parent bodies.

The current classification scheme contains 50 groups (Weisberg et al., 2006). In addition, there are a number of ungrouped meteorites that derive from parent bodies that are not represented by these groups. This number can be roughly estimated to be a maximum of 50

distinct parent bodies for ungrouped iron meteorites, and a maximum of 50 for ungrouped chondrites, based on the Meteoritical Bulletin Database. The total number of asteroids represented in the global meteorite collection is thus about 150 at most. A similar estimate of ~110 asteroids was reached based on consideration of oxygen isotopes (Greenwood et al., 2017). A more recent estimate, also based on consideration of oxygen isotopes, places the number of parent bodies between 95 and 148 (Greenwood et al., 2020). In this total, the number of chondrite parent bodies is estimated to be approximately 15 to 20, with an additional 11 to 17 parent bodies to account for ungrouped chondrites (Greenwood et al., 2020). Whatever the exact number of parent bodies represented in the global meteorite collection, it is almost negligible compared to the number of asteroids in the main belt, over one million asteroids larger than 1 km (Burbine et al., 2002). This suggests at first sight that meteorites are not representative at all of the asteroid population. However, asteroids were formed as bodies > ~35 km (Delbo et al., 2017). The smaller asteroids in the present-day asteroid belt belong to dynamical families and thus represent fragments of a small number (several dozens) of shattered planetesimals (Delbo et al., 2017). In addition to these fragments, the asteroid belt contains a small number (about a hundred) of pristine planetesimals with a diameter above ~35 km (Delbo et al., 2017). Therefore, with about 150 groups, meteorites may provide a rather exhaustive sampling of the planetesimals (shattered and pristine) that are present today in the asteroid belt. This justifies paying particular care to the grouping of meteorites into groups that actually originate from distinct primary parent bodies, especially for chondrites that are distributed within only 15 groups. Deciphering the parent body history, in terms of accretion (timing and physico-chemical environment) and evolution (thermal metamorphism and possible differentiation, aqueous alteration, and shock histories), also requires that the classification scheme efficiently separates groups of meteorites that were formed on different parent bodies.

CV chondrites are a fairly abundant type of carbonaceous chondrites with 525 meteorites registered by the Meteoritical Society to date (21% of the total number of carbonaceous chondrites). They are classically interpreted as coming from a single parent body (e.g., Krot et al, 1995). They have been divided into reduced (CV_{Red}) and oxidized (CV_{Ox}) sub-groups, based on a number of mineralogical features, the Ni content of sulfides and the abundance of Fe,Ni metal (McSween, 1977). The oxidized sub-group has been further divided into Allende- (CV_{OxA}) and Bali- (CV_{OxB}) like sub-groups, based on a combination of chemical and petrographic criteria (e.g., Krot et al., 1998; Bonal et al., 2020). Although an in-depth discussion of relations between CK and CV chondrites is beyond the scope of this paper, we note that it had also been proposed that CK chondrites may come from a more thermally metamorphosed (deeper) part of the same CV parent body based on compositional and oxygen isotope evidence (e.g., Wasson et al., 2013; Greenwood et al., 2010). On these bases, it was proposed to make CK chondrites a new sub-group of CV chondrites named CV_{OxK} (Greenwood et al., 2010). However, this interpretation has been later challenged by the different magnetite composition (Dunn et al., 2016) and the different chromium isotopic composition between CV and CK (Yin and Sanborn, 2019).

The present-day paradigm is that all CV chondrites come from a single parent asteroid, with a common protolith affected by significant parent body fluid-assisted metasomatism occurring at different temperatures and/or redox conditions (Krot et al., 1995; Ganino and Libourel, 2017). In this work we will argue that although CV_{OxA} and CV_{OxB} are likely to originate from a single parent body, CV_{Ox} and CV_{Red} originate from two distinct parent bodies.

2. Material and methods

We investigated a suite of 53 CV chondrites. The main dataset is composed of 30 meteorites (7 falls and 23 finds, mostly from Antarctica) whose thermal metamorphism and aqueous alteration history, matrix abundances, modal metal abundances, and sub-classification into CV_{OxA}, CV_{OxB}, and CV_{Red} have been characterized previously (Bonal et al., 2020). This dataset was completed by 23 meteorites from hot deserts, mostly from Northwest Africa (NWA meteorites). For this new set of meteorites, we determined the sub-group (OxA, OxB or Red) by combining proxies (mostly the average Ni content of sulfides, the Fe,Ni metal abundance, and magnetic parameters) that have been shown to allow for a clear separation of the three sub-groups (Bonal et al., 2020). We also estimated the modal abundance of fine-grained matrix. We then estimated the apparent chondrule diameters for all 53 meteorites. For a subset of samples, we measured the bulk oxygen isotopic composition by laser fluorination coupled with isotope-ratio mass spectrometry.

The chemical compositions of sulfides and Fe,Ni metal were determined using either a Cameca SX100 electron microprobe at CAMPARIS facility (15 kV accelerating voltage, 10 nA current), or a Hitachi S3000-N Scanning Electron Microscope equipped with a Bruker X-ray Energy Dispersive Spectrometer at CEREGE. Both natural and synthetic standards were used for calibration.

Magnetic susceptibility (χ) was measured at CEREGE, using a MFK1 apparatus from Agico in an AC field of 200 $A.m^{-1}$ (peak field) and frequency 976 Hz. For easiness, it is expressed in the following as $\log\chi$, with χ in 10^{-9} m^3/kg.

Chondrule apparent diameters were determined from mosaic images obtained by reflected and/or transmitted light microscopy on thin and/or thick polished sections using a Leica DM2500P microscope. Intact chondrules were outlined manually. Igneous chondrule rims, that are abundant in CV chondrites (Rubin, 1984), were included in the chondrule outline since they are obviously a pre-accretionary feature. The chondrule outlines were processed

using imageJ software and fitted with ellipses to extract chondrule apparent diameters. Most chondrules are not spheres but ellipsoids, giving an ellipse rather than a circle when observed in section. The maximum and minimum axes of the ellipses, noted a and b, were determined to estimate the aspect ratio of the chondrule. Chondrule apparent diameter was computed as $\sqrt{a.b}$, which is the diameter of the circle with equivalent surface to the observed chondrule. This method is slightly different from the simple averaging of a and b that is used classically in the literature (e.g., Nelson and Rubin, 2002) and provide systematically higher diameter estimates. However, the difference between the two methods is negligible (less than 1% for the typical aspect ratios observed in CV chondrules), so our results can be safely compared with literature data. Because chondrules are igneous fragments with almost no initial porosity, their volume will not change upon deformation. Our method therefore provides a more reliable estimate of the initial diameter of the initially spherical chondrules.

Modal metal abundances were determined by reflected light optical microscopy on polished sections by point-counting using a x500 magnification and a step size of 100 µm. The modal abundances of fine-grained matrix were determined by reflected and transmitted light optical microscopy on polished and thin sections by point-counting using a x200 magnification and a step size of 100 µm. The 95% confidence intervals around the modal abundances were computed after Howarth (1998).

Measurements of oxygen isotopic compositions of 1.5 mg aliquots of bulk gently powdered CV meteorites were carried out at the Stable Isotopes Laboratory of CEREGE using laser fluorination coupled with isotope ratio mass spectrometry (IRMS) (see e.g., Alexandre et al., 2006; Suavet et al., 2010 for more details about the analytical procedure). The initial sample mass was 112 mg on average to ensure that measured aliquot is representative of the bulk meteorite. The three oxygen isotopic compositions were measured with a dual-inlet mass spectrometer ThermoScientific Delta V plus. The oxygen isotope

results are expressed in ‰ versus the international reference standard V-SMOW: $\delta^{18}O = [(^{18}O/^{16}O)_{sample}/(^{18}O/^{16}O)_{V\text{-}SMOW}\text{-}1]\times1000$ and $\delta^{17}O = [(^{17}O/^{16}O)_{sample}/(^{17}O/^{16}O)_{V\text{-}SMOW}\text{-}1]\times1000$. The $\delta^{18}O$ and $\delta^{17}O$ values of the reference gas were calibrated with measurements of NBS28 standard ($\delta^{18}O$=9.60‰, Gröning, 2004). The $\delta^{17}O$ value of the NBS28 standard is taken as $\delta^{17}O$ =4.992‰, to ensure $\Delta^{17}O$= 0‰, where $\Delta^{17}O = \delta^{17}O - 0.52\times \delta^{18}O$. The measurements were corrected on a daily basis using 1.5 mg quartz internal laboratory standard "Boulangé" (Alexandre et al., 2006; Suavet et al., 2010). During the analyzing period, the analytical uncertainties derived from repeated measurement (n = 16) of this internal laboratory standard are 0.08 ‰, 0.14 ‰, 0.013 ‰ for $\delta^{17}O$, $\delta^{18}O$ and $\Delta^{17}O$, respectively.

A number of datasets were compared using the Kolmogorov-Smirnov (K-S) statistical test for two populations performed using Holliday (2017). The K-S test is used to tests the null hypothesis that the two data sets are from the same distribution. It provides a p value that must be compared to the *a priori* level of significance (α). If $p>\alpha$, the null hypothesis cannot be rejected. If $p<\alpha$, the null hypothesis is rejected. The significance level α has a specific meaning: it is the probably of rejecting the null hypothesis when it is true. α is classically set at 0.05, and we use this value in this work.

3. Results

All meteorites could be readily classified into one of the three sub-groups (Ox_A, Ox_B, Red), based mostly on the Ni content in sulfides and their magnetic susceptibility (Table 1, Figure 1). Unlike for fresh Antarctic meteorites and falls, the modal metal abundance in hot desert meteorites is not a reliable proxy for the separation into the three subgroups because metal is extensively altered into oxides and oxyhydroxides through terrestrial weathering during the residence of the meteorites in hot deserts. Magnetic susceptibility remains

nevertheless a reliable proxy to separate CV_{OxA} from CV_{OxB}. Indeed, although terrestrial weathering of metal-bearing meteorites does result in a decrease of magnetic susceptibility (e.g., Rochette et al., 2003), it does not affect magnetite which is the main ferromagnetic mineral in CV_{Ox}. Therefore, the cut-off value at $\log\chi$=3.9-4 for separation of CV_{OxA} from CV_{OxB} remains valid. On the contrary, the susceptibility of hot desert CV_{Red} is lower on average than that measured for falls and Antarctic CV_{Red}, with $\log\chi$=4.12 ± 0.45 (n=10) against 4.36 ± 0.22 (n=5) for Antarctic CV_{Red} and 4.52 ± 0.22 (n=3) for CV_{Red} falls (Rochette et al., 2008; Bonal et al,. 2020). But CV_{Red} are easily distinguished from CV_{Ox} based on the average Ni content of sulfides.

The 23 CV3 chondrites from hot deserts separate into 4 CV_{OxA}, 9 CV_{OxB}, 10 CV_{Red}. Together with the 30 meteorites studied in Bonal et al. (2020), the dataset comprises 14 CV_{OxA}, 20 CV_{OxB}, 19 CV_{Red}. The number of CV_{OxB} goes down to 18 when considering the pairing of Antarctic meteorites proposed by Bonal et al. (2020).

A total of 2806 chondrule apparent diameters were measured (Table 1). We did not attempt any correction to calculate a true (3D) size distribution from the 2D apparent size because it has been shown that many correction models yield erroneous values and should not be applied to chondrule size distributions (Metzler, 2018). Average values for the three sub-groups are given in Table 2. Although the chondrule diameters of all CV chondrites are usually pooled together to indicate an approximate mean apparent diameter of 900 µm (Friedrich 2015), our data show that CV chondrites actually have an average diameter of 801 µm (n=2806). Moreover, CV_{Red} meteorites have, on average, larger chondrules than CV_{Ox} meteorites (860 µm versus 768 µm). The size distributions of the sub-groups were compared using the K-S test (Table 3, Figure 2). The hypothesis that the chondrule size distributions of CV_{OxA} and CV_{OxB} are different cannot be rejected ($p = 0.056 > \alpha = 0.05$), whereas the chondrule size distributions of CV_{Red} and CV_{Ox} are different ($p = 6.78 \times 10^{-10} < \alpha = 0.05$).

Matrix modal abundances are also different between CV_{Ox} and CV_{Red} meteorites with average values 52.3 vol. % and 40.3 vol. %, respectively (Table 2). Their distributions were compared using the K-S test (Table 3). With $p=1.23x10^{-4}$, the matrix abundance distributions of CV_{Red} and CV_{Ox} are different. Conversely, the distributions of matrix abundances in CV_{OxA} and CV_{OxB} cannot be distinguished at the 5% significance level ($p = 0.295 > \alpha = 0.05$).

Oxygen isotopes were measured in this study for 17 CV chondrites (Table 4). Literature data are available for another 56 CV chondrites (Table 5, Figure 3), but most of these chondrites are not subclassified into CV_{Red} and CV_{Ox}. It has been noted earlier that CV chondrite can have heterogeneous oxygen isotopic composition (Greenwood et al., 2010). This is attributable to the small mass analyzed (usually in the mg range), combined with the size of their petrographic components: chondrules, calcium-aluminum inclusions (CAIs) and matrix lumps can be mm-sized and have widely variable oxygen isotopic composition (Clayton and Mayeda, 1999). In this study, we started from as large as possible bulk samples before analyzing a 1.5 mg aliquot. To reduce this homogeneity issue, when multiple analyses are available from the literature and our analyses, we use the average value (Table 5). Combining our new data and literature data, oxygen isotopic composition is available for 7 CV_{OxA}, 10 CV_{OxB}, 4 CV_{Ox}, and 16 CV_{Red}. In a three-isotope plot, the data are distributed along a line with slope 0.94 (Clayton, 1993), called the carbonaceous chondrite anhydrous mineral (CCAM) line. Therefore, the discussion can be limited to either $\delta^{18}O$ or $\delta^{17}O$. The distributions of $\delta^{18}O$ for the three sub-groups were tested using the K-S test. Again, the hypothesis that CV_{Red} and CV_{Ox} have identical distributions can be rejected at the 5% significance level ($p = 6.0x10^{-5} < \alpha = 0.05$), whereas CV_{OxA} and CV_{OxB} distribution cannot be distinguished at the same significance level ($p = 0.117 > \alpha = 0.05$). This latter observation contradicts previous observations that CV_{OxB} have a heavier oxygen isotopic than CV_{OxA} (Clayton and Mayeda, 1999; Greenwood, 2010), which was interpreted as more extensive

225 aqueous alteration in CV_{OxB} than in CV_{OxA}. We attribute this discrepancy to the more limited
226 dataset used in previous studies.
227
228 **4. Discussion**
229 The distribution of matrix abundances and chondrule apparent diameters are identical for
230 CV_{OxA} and CV_{OxB} chondrites but significantly different between CV_{Ox} and CV_{Red} chondrites.
231 Regarding chondrule apparent diameter, it is noteworthy that chondrules are usually not
232 spherical but ellipsoidal. This flattening, also observed at microscopic scale (Bland et al.,
233 2011) is likely due to hypervelocity impacts (e.g., Gattacceca et al., 2005). However, the
234 larger apparent chondrule diameters of CV_{Red} compared to CV_{Ox} cannot be attributed to the
235 effect of chondrule flattening. First, CV_{Red} chondrules are only slightly more flattened than
236 CV_{Ox} chondrules, with average aspect ratio 1.33 and 1.27, respectively (Table 2). Second, we
237 estimated the effect of the flattening of spherical chondrules into oblate ellipsoids on the
238 average apparent surface of the chondrules in polished sections (Supplementary figure S1).
239 This was done using an analytical solution for the intersection of plane and ellipsoids (Klein,
240 2012). The effect is a decrease of the apparent surface for increasing flattening. The effect is
241 small (about 0.5% average apparent diameter decrease for an aspect ratio of 1.35), and more
242 importantly it is the opposite of what is observed: CV_{Red} are slightly more flattened on
243 average than CV_{Ox}, but they have larger chondrules. The difference in chondrule size
244 distribution between CV_{Ox} and CV_{Red} is therefore a primary feature from the time of
245 accretion, and is not related to secondary parent body processes (shock).
246 Regarding matrix abundance, it is noteworthy than hypervelocity impacts will reduce
247 matrix porosity (e.g., Bland et al., 2011; Rubin, 2012) and reduce its modal abundance
248 compared to chondrules that have sub-null initial porosity. However, although it often
249 assumed that CV_{Red} are more shocked than CV_{Ox} on average based on a very limited number

of unusually shocked CV_{Red} (mostly Leoville and Efremovka), it has been shown recently that this is not the case. Indeed, shock stages for CV_{Ox} and CV_{Red} have essentially the same distribution (Bonal et al., 2020). This is confirmed here by the almost identical chondrule apparent aspect ratio for CV_{Red} and CV_{Ox} (Tables 1 and 2). Therefore, the difference in matrix abundance distribution between CV_{Ox} and CV_{Red} is also a primary feature from the time of accretion.

These two robust petrographic indicators (chondrule size and matrix abundance) can be interpreted in two different ways: CV_{Ox} and CV_{Red} originate from different stratigraphic position within a single parent body, or from two distinct parent bodies. Different stratigraphic positions in an asteroid with "onion-shell" structure would imply contrasted metamorphic temperatures with the deeper group being metamorphosed to higher temperatures. This is not observed, as both CV_{Ox} and CV_{Red} meteorites span the whole range of type 3 metamorphic subtypes (Bonal et al., 2020). Therefore, CV_{Ox} and CV_{Red} meteorites must originate from two different parent bodies. The existence of CV_{Ox} clasts in Vigarano CV_{Red} regolith breccia (Krot et al., 2000), often used as an evidence for a single parent body is not a decisive argument as xenolithic clasts from different meteorite groups are found in a number of meteorites. About 5% of impacts in the main asteroid belt should occur at velocities that are below the estimated survivable impact velocity for stony meteorites (Bottke et al., 1994; Bland, 2001), so that chondritic xenoliths are expected in chondrites, especially for chondrites from the same clan that are interpreted to come from parent bodies located at similar heliocentric distances. For instance, several ordinary chondrites contain cm-size clasts from another ordinary chondrite group (e.g., Gattacceca et al., 2017).

CV_{OxA} and CV_{OxB} cannot be distinguished in terms of chondrule size and matrix abundance. As such they may well originate from the same parent body. It was recently evidenced that CV_{OxA} are systematically more metamorphosed than CV_{OxB}, with a continuum

275 spanning all the petrographic subtypes 3.0 to ≥3.7 (Bonal et al., 2020). Such a distribution of
276 metamorphic grades is very unlikely to be casual and strongly suggests that indeed, CV_{OxA}
277 represent deeper level than CV_{OxB} in a single and thermally stratified parent body. A potential
278 counter-argument is that experimental data show that dehydration by heating of a
279 phyllosilicate-bearing rock should result in a shift towards heavier oxygen isotopic
280 composition (Mayeda and Clayton, 1998). Such a trend is not seen in the oxygen isotopic
281 distributions of CV_{OxA} and CV_{OxB}, that cannot be distinguished by the K-S test. However,
282 CV_{Ox} chondrites are complex rocks with only a minor fraction of phyllosilicates, a few wt.%
283 at most (Bonal et al., 2020), so that the effect of dehydration of phyllosilicates during thermal
284 metamorphism would not be significant compared to the natural inhomogeneity of oxygen
285 isotopic composition of CV chondrites discussed above.

286 The difference between CV_{Red} and CV_{Ox} in terms of oxygen isotopic composition may be a
287 primary feature acquired at the time of accretion, or a secondary parent body feature. A parent
288 body origin can be tested by assuming an original identical oxygen isotopic composition later
289 modified by aqueous alteration and/or thermal metamorphism. We tested the correlation
290 between $\delta^{18}O$ and quantitative proxies describing aqueous alteration and thermal
291 metamorphism (Figure 4). For aqueous alteration we use the total mass loss between 200 and
292 900 °C during thermogravimetric analyses (TGA) that increases with increasing hydration of
293 the meteorite. For thermal metamorphism, we use the Raman spectral parameter $FWHM_D$ that
294 decreases with increasing peak metamorphic temperature. The TGA and Raman parameters
295 are from Bonal et al. (2020). We see no correlation between $\delta^{18}O$ and TGA parameters
296 (R^2=0.007), suggesting no straightforward influence of aqueous alteration on the oxygen
297 isotopic composition of CV chondrites. There is a correlation between $\delta^{18}O$ and the Raman
298 spectroscopy parameter $FWHM_D$ (R^2=0.27, Figure 4). Such a correlation suggests that higher
299 metamorphic temperatures result in heavier oxygen isotope compositions. This can be

accounted for by the effects of metamorphic heating, such as recrystallization or dehydration, that would result in an increase of $\delta^{18}O$ by mass fractionation. But the observed correlation is faint (R^2=0.27), and it does not hold at all if we consider CV_{OxA} and CV_{OxB} subgroups. Eventually, we find no robust correlation between the peak metamorphic temperature or the degree of aqueous alteration, and the oxygen isotopic composition of CV chondrites: no global parent body processes is able to account for the observed distribution of oxygen isotopic compositions in CV_{Ox} and CV_{Red} chondrites. Therefore, the difference in isotopic composition between CV_{Red} and CV_{Ox} is more likely controlled by subtle differences in the abundances of petrographic components (matrix, chondrules, CAIs for instance), or by accretion at slightly different distances from the Sun implying reservoirs with slightly different oxygen isotopic compositions.

Cosmic ray exposure (CRE) ages, that represent the transit time of a meteorite (under the form of a meteoroid) from the asteroid belt to the Earth are another useful proxy in the discussion about whether different meteorites may originate from a single parent body. Similar CRE ages may indicate provenance from the same parent body affected by a major disruption event. However, the dataset of CRE ages for CV chondrites is limited to 4, 5, and 3 ages available for CV_{OxA}, CV_{OxB} and CV_{Red}, respectively (Schere and Schultz, 2000). The three sub-groups span broadly the same time interval of CRE ages between 1.7 and 28.1 Ma, with average CRE ages 16.0 ± 7.8 Ma (n=4) for CV_{OxA}, 11.0 ± 9.4 Ma (n=5) for CV_{OxB}, 13.2 ± 9.1 Ma (n=9) for all CV_{Ox}, and 8.6 ± 2.2 Ma (n=3) for CV_{Red}. Because of the limited dataset, CRE ages cannot be used to discuss the hypothesis of a single or multiple parent bodies for CV chondrite sub-groups.

We have demonstrated that CV_{Red} and CV_{Ox} meteorites come from two distinct parent bodies. Because the ultimate goal in chondrite classification is that a chondrite group represents one parent body, CV_{Red} and CV_{Ox} should be separated into two proper groups.

Chondrite groups are classically, but not systematically, named after the first fall of the group. Strictly speaking, the CV appellation, that comes from Vigarano CV_{Red} fall, should be applicable only to CV_{Red} chondrites, and an alternative name should be defined for CV_{Ox} chondrites. Such a name could be CA for the iconic Allende meteorite, because all other CV_{Ox} fall names (except Grosnaja) initiate with letters already in use for other meteorite groups. However, because there are already thousands of scientific publications about Allende and other CV_{Ox} meteorites calling them CV, it very likely that such an appellation would encounter strong resistance from the meteorite community. Therefore, the best names for these two separate meteorite groups are probably simply CV_{Ox} and CV_{Red}, where the reference to Vigarano remain somewhat valid since this meteorite contains material from both associated parent bodies. We hope that from now on, CV chondrites will be required to be declared to the Meteoritical Society as CV_{Ox} or CV_{Red}, and not only as CV. On the other hand, the distinction between CV_{OxA} and CV_{OxB} is only related to thermal metamorphic intensity and could be overlooked in the classification scheme.

On a practical point of view, the easiest and most robust way to separate CV_{Red} and CV_{Ox} is to estimate the average Ni content of sulfides. Indeed, in contrast to metal abundance or magnetic parameters, this indicator is not much affected by terrestrial weathering. Analyses of a random selection of about 10 to 20 sulfide grains is enough to decide between CV_{Red} and CV_{Ox} and can be performed routinely during classification work using either an electron microprobe or a scanning electron microscope equipped with an energy dispersive spectrometer.

5. Conclusions

The comparison of chondrule size distribution, matrix abundances, metamorphic history (and marginally oxygen isotopic composition) of the three sub-groups of CV chondrites

indicate that CV_{Red} and CV_{Ox} originate from distinct parent bodies. In view of the many petrographic, compositional and isotopic similarities between CV_{Ox} and CV_{Red}, these two parent bodies may have however formed at roughly the same heliocentric distance and time.

On the other hand, CV_{OxA} and CV_{OxB} likely originate from the same parent body, with CV_{OxA} representing deeper, more metamorphosed levels of the original asteroid with onion-shell structure. This new view must be considered in future works about the formation and evolution of these two parent bodies, as results (existing and to come) must be interpreted in two separate frameworks.

For clarification of the chondrite classification scheme, in which one group should represent a parent body, we propose to break the CV group into two proper groups (and not subgroups as is the current scheme), keeping the names CV_{Red} and CV_{Ox}. These two groups can be readily separated by estimating the average nickel content of their sulfides.

Acknowledgements

We thank two anonymous reviewers for their constructive comments. We thank Yoann Quesnel for coding the computation of the effect of flattening on chondrule apparent diameters. We thank Jeff Grossman for useful discussion about meteorite nomenclature.

Figure captions

Figure 1: Ni content of sulfides versus magnetic susceptibility for the CV chondrites studied in this work. Light blue=CV_{OxA}, deep blue=CV_{OxB}, red =$CV_{Red.}$ Circles are for hot desert meteorites (this study), squares are for Antarctic meteorites and falls (Bonal et al., 2020).

Figure 2: Cumulative percentile plots for apparent chondrule size, matrix abundance and $\delta^{18}O$. Light blue = CV_{OxA}, deep blue=CV_{OxB}, black=CV_{Ox}, red=CV_{Red}.

Figure 3: Oxygen isotopic composition of CV chondrites. The CCAM line is from Clayton (1993).

Figure 4: Oxygen isotopic composition versus (a) the total mass loss as measured by TGA between 200 and 900 °C, (b) the Raman spectral parameter $FWHM_D$. The TGA parameters reflects the present-day hydration state of the samples, while the Raman parameters the experienced peak metamorphic temperature. Light blue = CV_{OxA}, deep blue=CV_{OxB}, red=CV_{Red}.

Supplementary figure S1: Effect of flattening on the average apparent diameters of chondrules. This graph shows the ratio of the average equivalent diameters (i.e., diameter of the disk with equivalent surface) of the of the intersection of ellipsoids with planes of random orientation as a function of the aspect ratio of these ellipsoids. To simulate the case of chondrules flattening by impacts, the case considered here is for oblate ellipsoids that have identical long and intermediate axis. The initial diameter considered here for normalizing the ellipsoid diameter assumes volume conservation during flattening.

Table captions

Table 1. CV chondrites physical, petrological and geochemical properties

Metal abundance: *tr* indicate that traces of metal have been observed. No polished section was available for GRA 06101. References: R2008= Rochette et al. (2008), B2020 = Bonal et al. (2020).

Table 2: Average properties of CV subgroups

Table 3: Kolmogorov-Smirnov test results.

N is the number of meteorites in the considered population. The hypothesis that the two distributions are identical can be rejected if $p > \alpha$. If $p < \alpha$, this hypothesis cannot be rejected. α is the significance level of the K-S test and is taken as 0.05 in this study.

Table 4: CV3 oxygen isotopic compositions measured in this study.

Table 5: summary of CV3 oxygen isotopic compositions. References: C&M1999= Clayton and Mayeda, 1999; G2010= Greenwood, 2010; MDB= Meteoritical Society Meteorite Database (https://www.lpi.usra.edu/meteor/).

References

Alexandre, A., Basile-Doelsch, I., Sonzogni, C., Sylvestre, F., Parron, C., Meunier, J.-D., Colin, F., 2006. Oxygen isotope analyses of fine silica grains using laser-extraction technique: Comparison with oxygen isotope data obtained from ion microprobe analyses and application to quartzite and silcrete cement investigation. Geochim. Cosmochim. Acta 70, 2827–2835.

Bland, P. A., 2001. Quantification of meteorite infall rates from accumulations in deserts, and meteorite accumulations on Mars. In Accretion of extraterrestrial matter throughout Earth's history, edited by Peucker-Ehrenbrink B. and Schmitz B. New York: Kluwer Academic/Plenum Publishers. pp. 267–303.

Bland, P.A., Howard, L.E., Prior, D.J., Wheeler, J., Hough, R.M., Dyl, K.A., 2011. Earliest rock fabric formed in the Solar System preserved in a chondrule rim. Nature Geoscience 4, 244-247.

Bonal, L., Gattacceca, J., Garenne, A., Eschrig, J., Rochette, P., Krämer Ruggiu, L., 2020. Water and heat: new constraints on the evolution of the CV chondrite parent body. Geochim. Cosmochim. Acta, 276, 363-383.

Bottke, W. F. Jr., Nolan, M. C., Greenberg, R., Kolvoord, R. A., 1994. Velocity distributions among colliding asteroids. Icarus 107, 255-268.

Burbine, T.H., McCoy, T.J., Meibom, A., Gladman, B., Keil, K., 2002. Meteoriticparent bodies: their number and identification. In: Bottke, W.F., Cellino, A.,Paolicchi, P., Binzel, R.P. (Eds.), Asteroids III. University of Arizona Press, Tucson, pp. 653–667.

Clayton, R. N., 1993. Oxygen isotopes in meteorites. Ann. Rev. Earth Planet. Sci. 21, 115-149.

Clayton, R.N., Mayeda, T.K., 1999. Oxygen isotope studies of carbonaceous chondrites. Geochim. Cosmochim. Acta 63, 2089–2104.

Delbo, M., Walsh, K., Avdellidou, C., Morbidelli, A., 2017. Identification of a primordial asteroid family constrains the original planetesimal population. Science 357, 1026-1029.

Dunn, T. L., Gross, J., Ivanova, M. A., Runyon, S. E., Bruck, A. M., 2016. Magnetite in the unequilibrated CK chondrites: Implications for metamorphism and new insights into the relationship between the CV and CK chondrites. Meteoritics Planet. Sci. 51, 1701-1720.

Eugster, O., Herzog, G.F., Marti, K., Caffee, M.W., 2006. Irradiation records, cosmic-ray exposure ages, and transfer times of meteorites, in Meteorites and the Early Solar System II, pp. 829-851.

Friedrich, J. M., Weisberg, M. K., Ebel, D. S., Biltz, A. E., Corbett, B. M., Iotzov, I. V., Khan, W. S., Wolman, M. D., 2015. Chondrule size and related physical properties: A compilation and evaluation of current data across all meteorite groups. Chemie der Erde 75, 419-443.

Ganino, C., Libourel, G., 2017. Reduced and unstratified crust in CV chondrite parent body. Nature Communications 8, 261.

Gattacceca, J., Krzesinska, A.M., Marrocchi, Y., Meier, M.M., Bourot-Denise, M., Lenssen, R., 2017. Young asteroid mixing revealed in ordinary chondrites: the case of NWA 5764, a polymict LL breccia with L clasts. Meteoritics Planet. Sci. 52, 2289-2304.

Gattacceca, J., Rochette, P., Denise, M., Consolmagno, G., Folco, L., 2005. An impact origin for the foliation of ordinary chondrites. Earth Planet. Sci. Lett. 234, 351-368.

Gravnik, M., Brown, P., 2018. Identification of meteorite source regions in the Solar System. Icarus 311, 271-287.

Greenwood, R.C., Franchi, I.A., Kearsley, A.T., Alard, O., 2010. The relationship between CK and CV chondrites. Geochim. Cosmochim. Acta 74, 1684-1705.

Greenwood, R.C., Burbine, T.H., Miller, M.F., Franchi, I.A., 2017. Melting and differentiation of early-formed asteroids: The perspective from high precision oxygen isotope studies. Chemie der Erde – Geochemistry 77,1-43.

Greenwood, R.C., Burbine, T.H., Franchi, I.A., 2020. Linking asteroids and meteorites to the primordial planetesimal population. Geochim. Cosmochim. Acta, doi: https://doi.org/10.1016/j.gca.2020.02.004

Gröning, M., 2004. Chapter 40 – International Stable Isotope Reference Materials. In Handbook of Stable Isotope Analytical Techniques. pp. 874–906.

Holliday, I.E., 2017. Kolmogorov-Smirnov Test (v1.0.4) in Free Statistics Software (v1.2.1), Office for Research Development and Education, URL https://www.wessa.net/rwasp_Reddy-Moores%20K-S%20Test.wasp/

Howarth, R.J., 1998. Improved estimators of uncertainty in proportions, point-counting, and pass-fail test results. American J. Sci. 298, 594-607.

Klein, P.P., 2012. On the ellipsoid and plane intersection equation. Applied Mathematics 3, 1634-1640.

Krot, A.N., Scott, E.R.D., Zolensky, M.E., 1995. Mineralogical and chemical modification of components in CV3 chondrites: Nebular or asteroidal processing? Meteoritics 30, 748-775.

Krot, A.N., Petaev, M.I., Scott, E.R.D., Choi, B.-G., Zolensky, M.E., Keil, K., 1998. Progressive alteration in CV3 chondrites: More evidence for asteroidal alteration. Meteoritics Planet. Sci. 33, 1065-1085.

Krot, A.N., Meibom, A., Keil, K., 2000. A clast of Bali-like oxidized CV material in the reduced CV chondrite breccia Vigarano. Meteoritics Planet. Sci. 35, 817-825.

Lee, M.R., Cohen, B.E., King, A.J., Greenwood, R.C., 2019. The diversity of CM carbonaceous chondrite parent bodies explored using Lewis Cliff 85311. Geochim. Cosmochim. Acta 264, 224-244.

McSween, H.Y., 1977. Petrographic variations among carbonaceous chondrites of the Vigarano type. Geochim. Cosmochim. Acta 41, 1777-1790.

Mayeda, T.K., Clayton, R.N., 1998. Oxygen isotope effects in serpentine dehydration. Lunar Planet. Sci. Conf. 29, abstract #1405.

Metzler, K., 2018. From 2D to 3D chondrule size data: Some empirical ground truths. Meteoritics Planet. Sci 53, 489-1499.

Nelson, V.E., Rubin, A., 2002. Size-frequency distributions of chondrules and chondrule fragments in LL3 chondrites: Implications for parent-body fragmentation of chondrules. Meteoritics Planet. Sci. 37, 1361-1376.

Rochette, P., Sagnotti, L., Bourot-Denise, M., Consolmagno, G., Folco, L., Gattacceca, J., Osete, M. L., Pesonen, L., 2003. Magnetic Classification of stony meteorites: 1. Ordinary chondrites. Meteoritics Planet. Sci. 38, 251-258.

499 Rochette, P., Gattacceca, J., Bonal, L., Bourot-Denise, M., Chevrier, V., Clerc, J.-P.,
500 Consolmagno, G., Folco, L., Gounelle, M., Kohout, T., Pesonen, L., Quirico, E.,
501 Sagnotti, L., Skripnik, A., 2008. Magnetic Classification of Stony Meteorites: 2. Non-
502 Ordinary Chondrites. Meteoritics Planet. Sci. 43, 959-980.
503 Rubin, A. E., 1984. Coarse-grained chondrule rims in type 3 chondrites. Geochim.
504 Cosmochim. Acta 48, 1779-1789.
505 Rubin, A. E. 2012. Collisional facilitation of aqueous alteration of CM and CV carbonaceous
506 chondrites. Geochim. Cosmochim. Acta 90, 181-194.
507 Scherer, P., Schultz, L., 2000. Noble gas record, collisional history, and pairing of CV, CO,
508 CK, and other carbonaceous chondrites. Meteorit. Planet. Sci. 35, 145-153.
509 Suavet, C., Alexandre, A., Franchi, I. A., Gattacceca, J., Sonzogni, C., Greenwood, R. C.,
510 Folco, L., Rochette, P., 2010. Identification of the parent bodies of micrometeorites with
511 high-precision oxygen isotope ratios. Earth Planet. Sci. Lett. 293, 313-320.
512 Wasson, J. T., Isa, J., Rubin, A. E., 2013. Compositional and petrographic similarities of CV
513 and CK chondrites: A single group with variations in textures and volatile
514 concentrations attributable to impact heating, crushing and oxidation. Geochim.
515 Cosmochim. Acta 108, 45-62.
516 Weisberg, M. K., McCoy, T. J., Krot, A. N., 2006. Systematics and evaluation of meteorite
517 classification. In Meteorites and the Early Solar System II, edited by Lauretta, Dante S.
518 and Sween Jr, H. Y., pp. 19-52.
519 Yin, Q.-Z., Sanborn, M.E., 2019. An update on disconnecting CV and CK chondrites parents
520 bodies and more. 50th Lunar Planet. Sci. Conf., abstract #3023.

Figure 1

Click here to download Figure: Fig1-classification.pdf

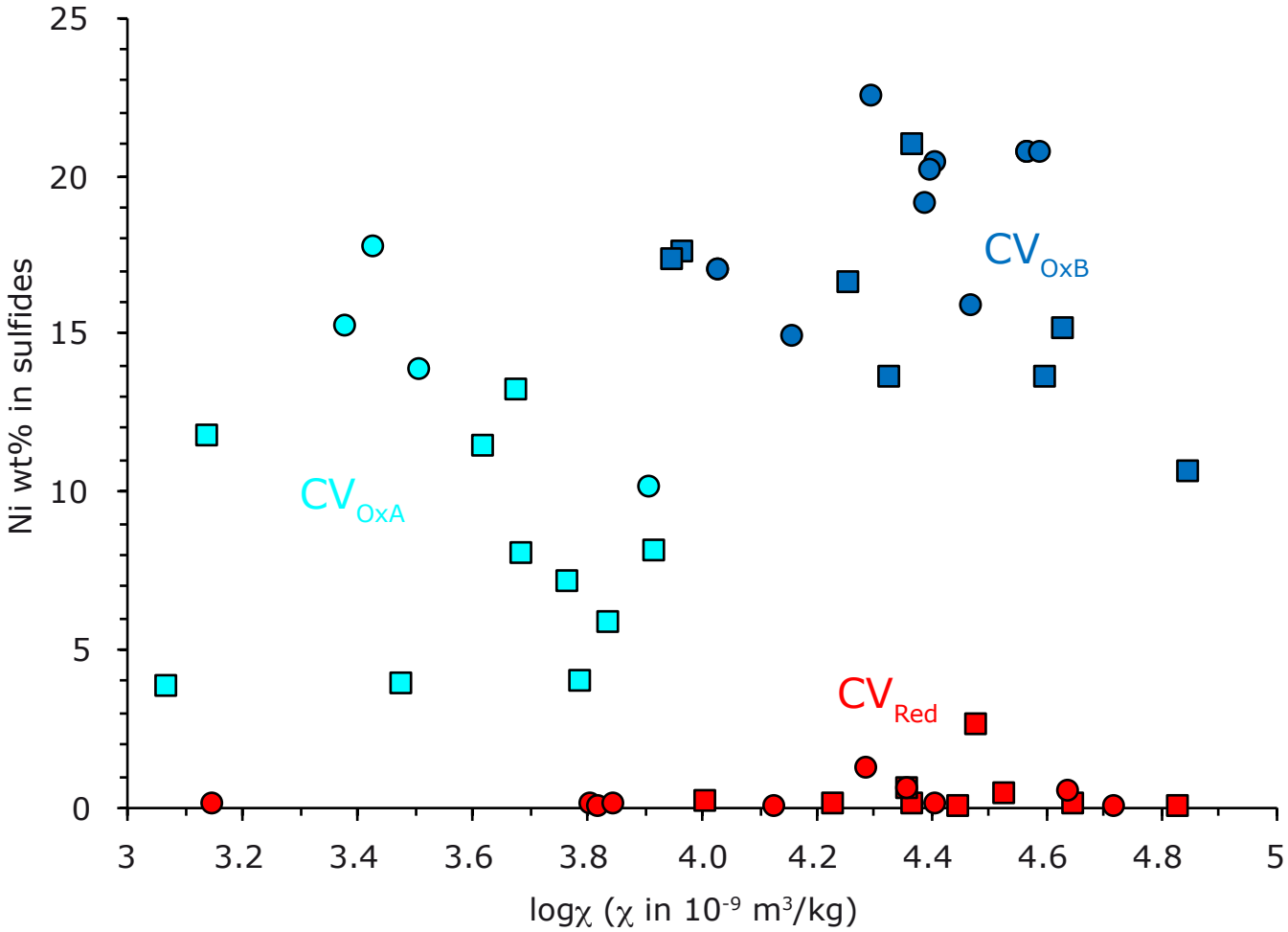

Figure 2

Click here to download Figure:1Fig2-cumulative plots.pdf

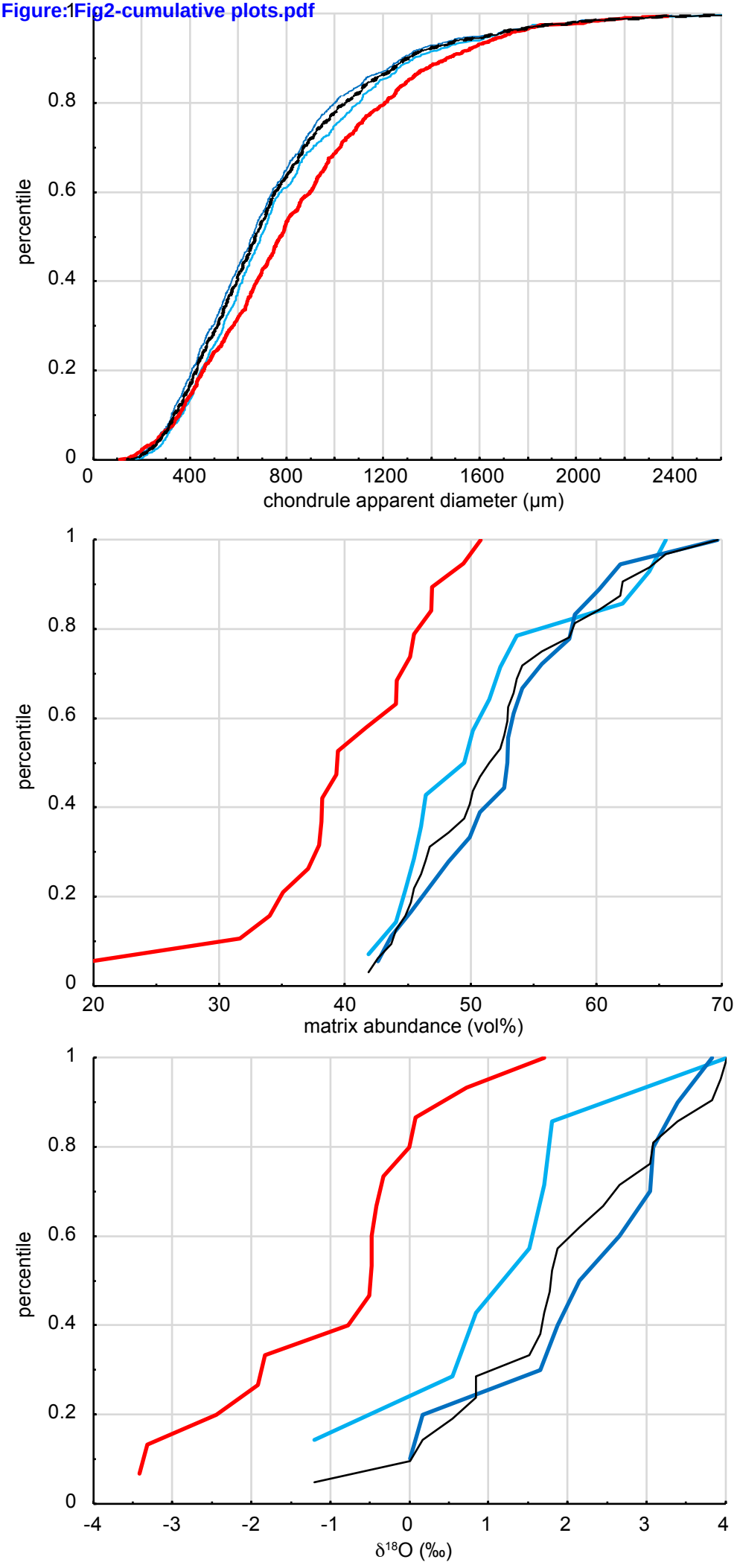

Figure 3

Click here to download Figure: Fig3-O isotopes.pdf

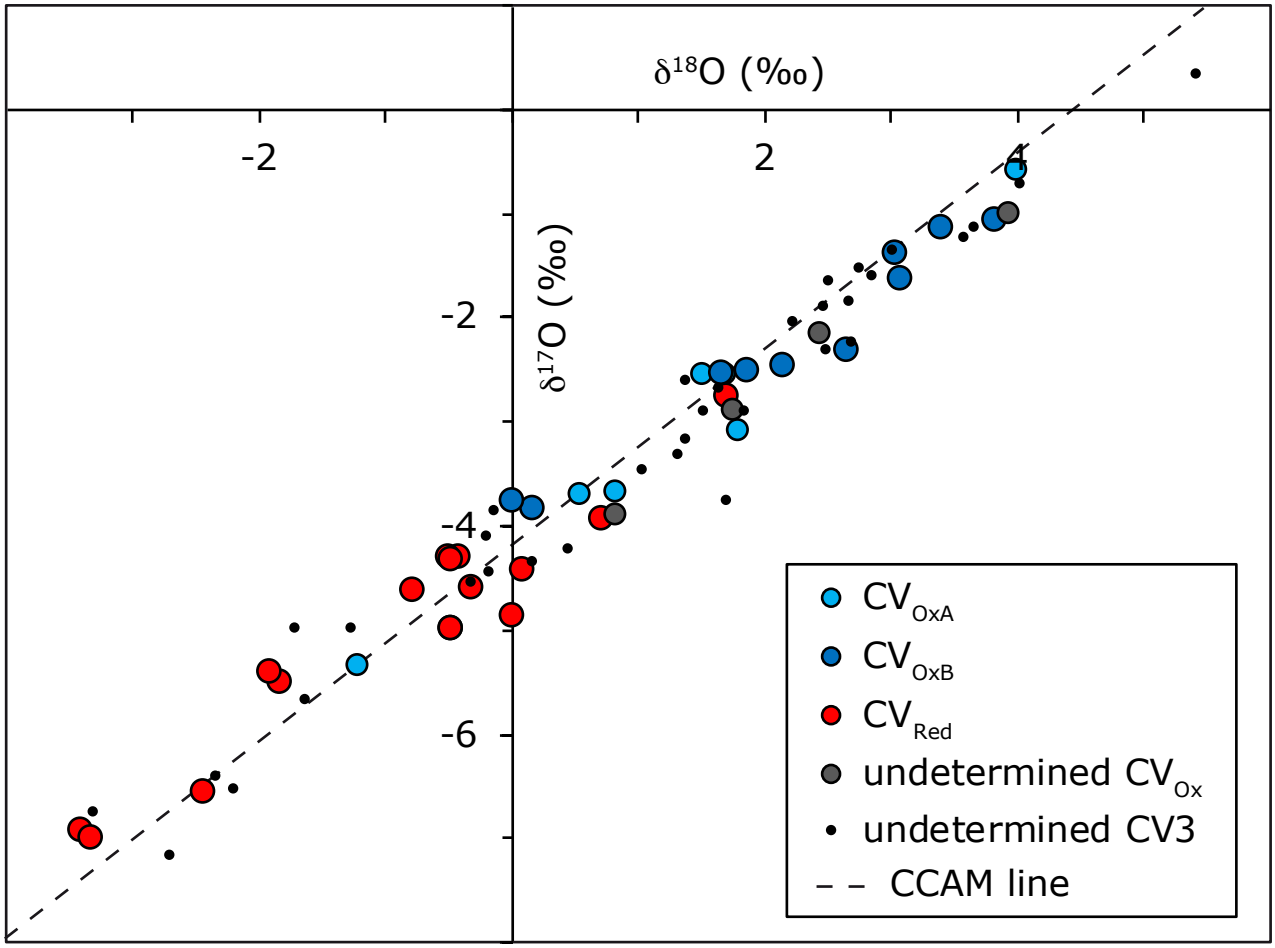

Figure 4b

Click here to download high resolution image

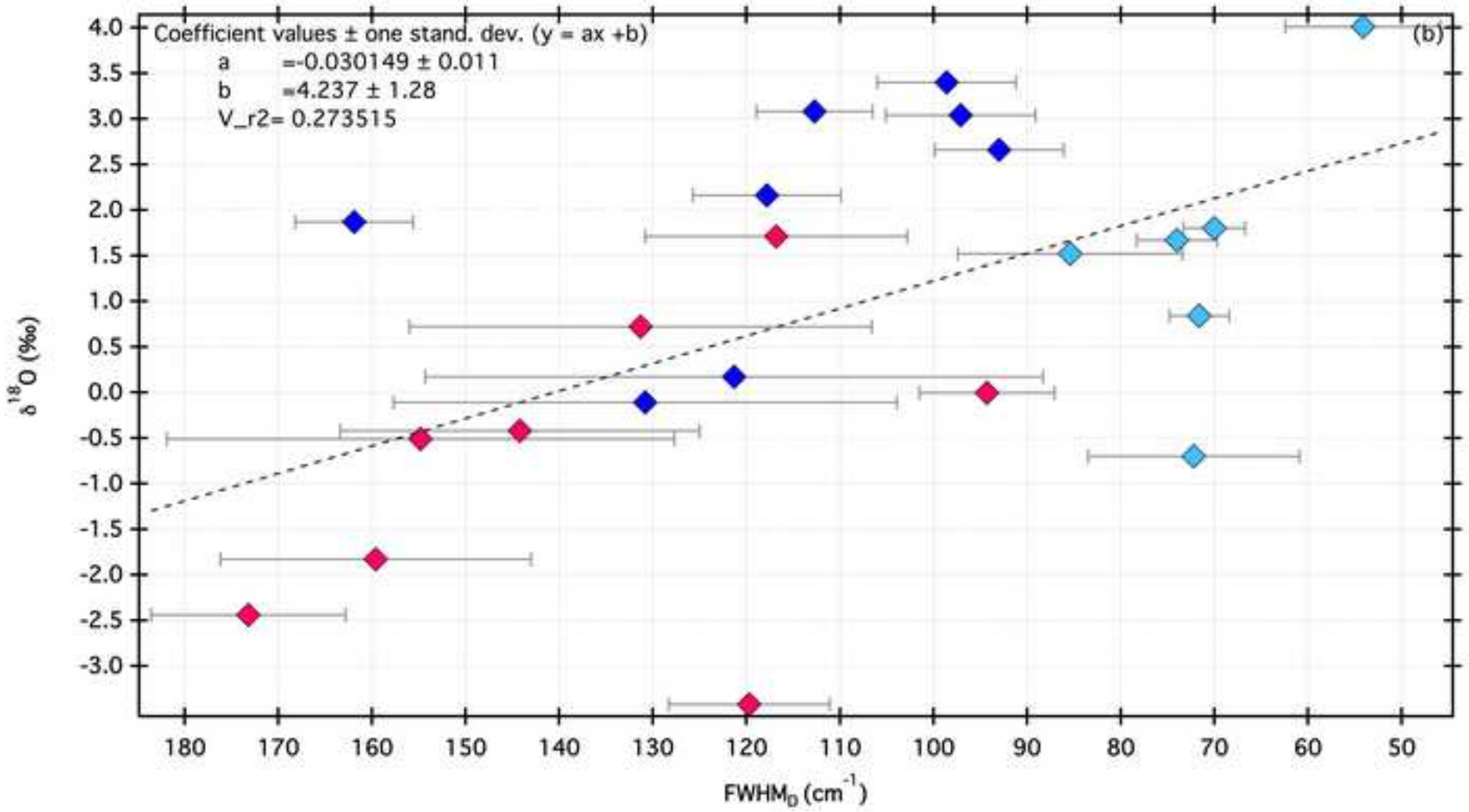

Figure 4a

Click here to download high resolution image

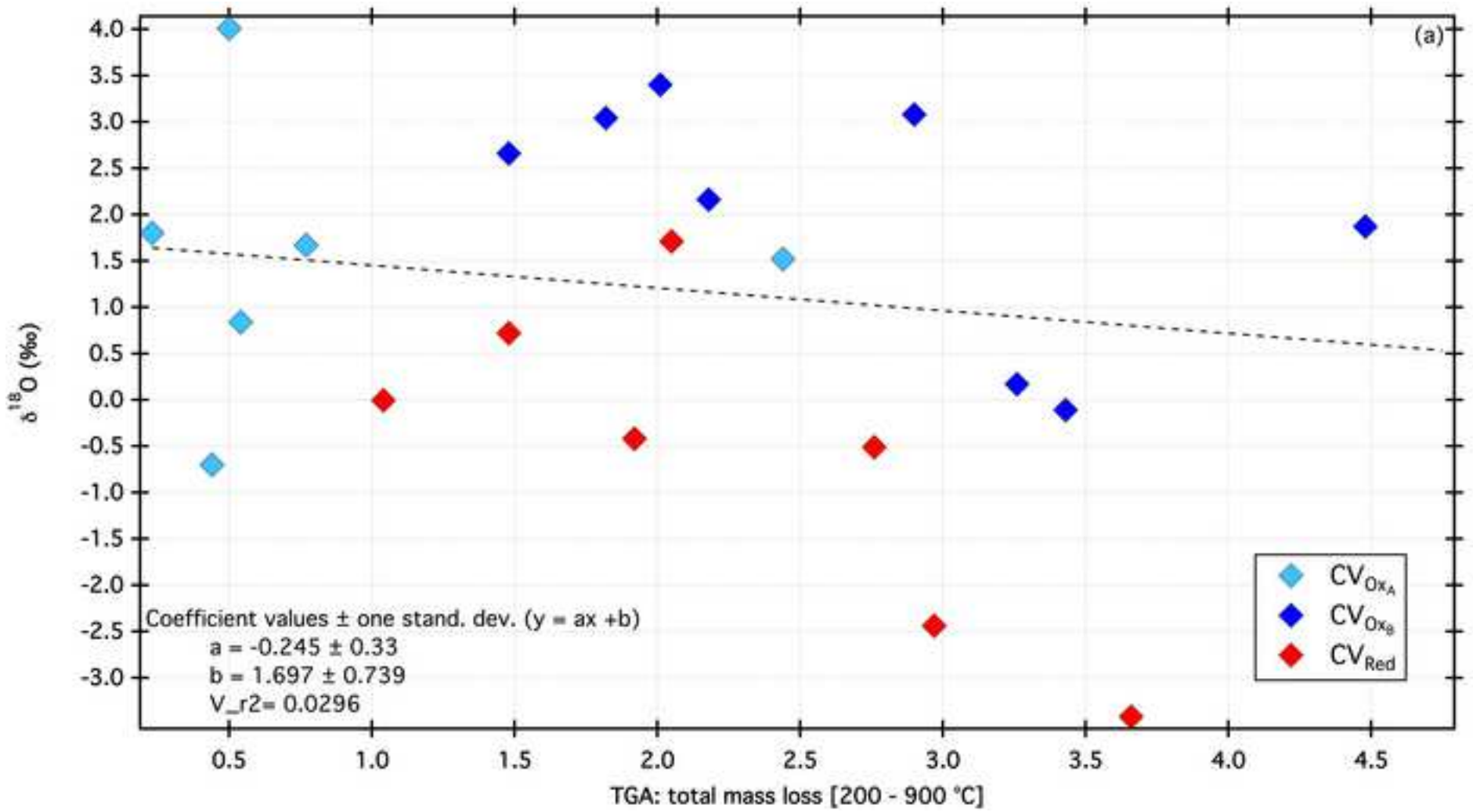

Table 1

Click here to download Table: Table 1-CV properties.xlsx

	matrix				Ni wt% in sulfides			Ni wt% in metal			Metal abundance					Magnetic susceptibility		Chondrule apparent diameter				
	abundance	surface cm2 / n	95% confidence lower bound	95% confidence upper bound	average	s.d.	n	average	s.d.	n	vol%	95% confidence lower bound	95% confidence upper bound	n	ref	logX	referece	average	s.d.	n	average aspect ratio	s.d.
CVOxA																						
ALH81003	54%	0.32			13.2	7.5	20	67.2	4.8	10	0.15%	0.14%	0.67%	676	B2020	3.68	R2008	423	217	5		
ALH84028	52%	1.72			8.07	10.66	20	66.3	1.1	4	1.01%	0.49%	0.75%	1192	B2020	3.92	R2008	772	356	102	1.3	0.24
Allende	50%	6.27			11.4	11.5	21	57.1	23	26	0.20%	0.16%	0.37%	1572	McS1977	3.62	R2008	765	406	134	1.18	0.13
Axtell	44%	1.95			11.7	9.8	7	67.5	1.4	2	0.00%	0.00%	1.11%	630	B2020	3.14	R2008	984	484	43	1.15	0.11
GRA06101																3.82	B2020					
GRA06130	50%	0.49			7.08	8.7	20	67.9	0.2	10	0.73%	0.46%	0.86%	818	B2020	3.77	B2020	801	442	21	1.25	0.16
LAP02206	45%	0.72			7.99	9.8	45	69.7	0.23	10	1.15%	0.47%	0.66%	1563	B2020	3.69	R2008	905	487	33	1.29	0.24
MIL07002	42%	1.00			3.93	6.1	20	66.5		1	0.54%	0.29%	0.48%	1664	B2020	3.79	B2020	846	445	57	1.29	0.21
MIL07671	46%	0.74			5.81	7.1	20	66.5	0.13	2	0.80%	0.43%	0.71%	1124	B2020	3.84	B2020	867	497	39	1.33	0.26
MIL091010	46%	1.21			3.89	6.7	20	67.8	0.5	15	0.28%	0.22%	0.53%	1084	B2020	3.48	B2020	1037	466	26	1.14	0.13
NWA 11087	46%	606	42%	50%	17.7	7.6	15	69.65		1	0.00%	0.00%	1.75%	400	this study	3.43	this study	772	310	50	1.2	0.12
NWA 11545	64%	631	60%	68%	13.8	10	3	70.4	3.4	3	0.00%	0.00%	1.40%	500	this study	3.51	this study	718	498	44	1.23	0.14
NWA 11589	52%	529	48%	57%	10.1	9.5	21	69.2	0.6	20	1.00%	0.40%	2.05%	701	this study	3.91	this study	735	498	50	1.19	0.11
NWA 12553	65%	455	61%	70%	15.2	8.4	15	68.2	0.4	5	0.10%	0.00%	0.57%	973	this study	3.38	this study	772	402	70	1.22	0.16
QUE94688	62%	0.76			3.78	5.37	22				0.09%	0.08%	0.40%	1143	B2020	3.07	R2008	924	405	25	1.32	0.25
CVOxB																						
ALH85006	48%	1.19			28.4	1.8	10				0.09%	0.09%	0.41%	1113	B2020	4.52	R2008	722	354	72	1.28	0.19
Bali	50%	3.35			16.6	5.9	20	16	14	2	0.00%	0.00%	0.33%	2103	McSween197	4.26	R2008	735	415	154	1.27	0.21
Catalina 300	53%	417	48%	58%	19.1	7.6	15				tr	0.00%	1.75%	400	this study	4.39	this study	756	500	87	1.3	0.2
Grosnaja	70%	1.52			17.5	8.2	15				0.00%	0.00%	0.37%	1885	McSween197	3.97	R2008	690	324	29	1.26	0.14
Kaba	53%	0.94			10.6	8.5	19	3.7	1.2	6	0.00%	0.00%	0.45%	1561	McSween197	4.85	R2008	715	309	40	1.19	0.12
LAR06317	60%	1.00			20.9	15.7	20				0.17%	0.17%	0.56%	1000	B2020	4.37	B2020	773	433	28	1.27	0.25
LAR06867	53%	0.70			17.3	10.1	20				0.19%	0.17%	0.47%	1102	B2020	3.95	B2020	707	362	25	1.22	0.13
MCY05219	54%	0.73			13.6	10.0	20				0.00%	0.00%	0.99%	704	B2020	4.33	B2020	665	220	18	1.2	0.17
MET00430/MET00761/MET01074	44%	2.29			15.1	7.6	20				0.00%	0.00%	0.77%	906	B2020	4.63	R2008	714	403	146	1.39	0.34
Mokoia	43%	0.34			13.6	6.6	18				0.00%	0.00%	0.46%	1510	McSween197	4.6	R2008	797	370	10	1.32	0.21
NWA 10162	58%	885	55%	62%	22.5	3.6	10				tr	0.00%	1.25%	561	this study	4.3	this study	746	450	79	1.35	0.21
NWA 10777	56%	390	51%	61%	20.1	5.5	15				tr	0.00%	1.40%	500	this study	4.4	this study	823	502	74	1.23	0.18
NWA 11533	45%	482	41%	50%	20.7	5.7	15				tr	0.00%	1.75%	400	this study	4.57	this study	864	453	94	1.24	0.16
NWA 11541	53%	502	49%	58%	17.0	0.7	7	55.9	1.6	3	tr	0.00%	1.47%	475	this study	4.03	this study	787	442	41	1.21	0.16
NWA 11546	58%	377	53%	63%	20.4	8	14				0.18%	0.00%	1.00%	554	this study	4.41	this study	682	383	53	1.29	0.24
NWA 12469	47%	507	42%	51%	20.7	1.9	15	54.9	25.5	14	tr	0.00%	1.75%	400	this study	4.59	this study	686	337	61	1.44	0.36
NWA 12959	62%	1.39			14.9	10.4	16				0.31%	0.04%	1.13%	636	this study	4.16	this study	831	330	31	1.43	0.18
Ramlat as Sahmah 531	51%	658	47%	55%	15.8	7.8	10	64.4	22.9	7	tr	0.00%	1.50%	465	this study	4.47	this study	594	444	50	1.24	0.12
CVRed																						
Bukhara	39%	1.45			0.05	0.2	10	27.7	20.3	25	2.23%	0.95%	1.37%	716	B2020	4.37	R2008	872	562	37	1.19	0.14
Efremovka	19%	1.18			0.00	0.0	15	1.6	2.5	30	4.60%	0.97%	1.14%	1611	McSween197	4.83	R2008	819	427	48	1.42	0.18
GRO95652	37%	0.75			0.05	0.1	10	27.1	19.6	10	3.12%	0.99%	1.28%	995	B2020	4.23	R2008	920	394	40	1.28	0.25
Leoville	32%	2.42			0.40	1.1	15	10.1	12.9	30	1.80%	0.59%	0.73%	1718	McSween197	4.53	R2008	1081	377	73	1.56	0.37
MIL07277	45%	0.90			0.07	0.2	30	20.7	18.2	25	4.10%	1.40%	1.85%	634	B2020	4.65	B2020	1149	665	19	1.54	0.32
NWA 11537	39%	497	35%	44%	0	0	10				0.20%	0.01%	1.11%	501	this study	4.72	this study	838	444	32	1.24	0.14
NWA 11543	46%	380	40%	51%	0.1	0.2	10				0.18%	0.00%	0.99%	560	this study	4.41	this study	696	475	86	1.21	0.15
NWA 12523	51%	453	46%	55%	0.1	0.2	7	35.9	1.7	15	1.86%	1.05%	3.05%	805	this study	3.81	this study	800	448	78	1.36	0.26
NWA 12554	47%	640	43%	51%	0.1	0.3	10				tr	0.00%	0.61%	1138	this study	3.15	this study	886	420	57	1.24	0.18
NWA 8331	44%	728	40%	48%	0.52	1.26	14	63.7	0.9	15	0.86%	0.43%	1.53%	1282	this study	4.36	this study	781	522	169	1.42	0.26
NWA 8445	42%	511	37%	46%	0.5	1.1	7				0.43%	0.05%	1.55%	462	this study	4.64	this study	1007	399	38	1.32	0.17
NWA 8478	38%	553	34%	42%	0.1	0.1	5				0.38%	0.05%	1.36%	529	this study	3.85	this study	881	456	34	1.3	0.21
NWA 8481	49%	591	45%	54%	0	0.1	10				0.50%	0.10%	1.45%	603	this study	3.82	this study	876	561	35	1.21	0.16
NWA 8483	47%	622	43%	51%	0	0	10				0.35%	0.04%	1.27%	568	this study	4.13	this study	867	450	63	1.3	0.22
QUE97186	44%	0.90			0.15	0.3	10	26.3	18.9	15	3.05%	1.13%	1.53%	721	B2020	4.01	R2008	1052	345	12	1.28	0.15
RBT04143	34%	1.47			2.60	7.1	43	29.3	19	28	1.66%	0.67%	0.95%	1087	B2020	4.48	B2020	917	345	56	1.44	0.3
RBT04302	38%	0.92			0.00	0.0	10	27.1	16.3	15	2.07%	0.82%	1.14%	920	B2020	4.45	B2020	952	711	24	1.26	0.16
Sueilila 003	38%	599	34%	42%	1.2	4.3	15	65	0.5	11	0.87%	0.35%	1.78%	807	this study	4.29	this study	748	397	52	1.25	0.21
Vigarano	35%	2.85			0.54	2.9	15	21.1	18.3	27	1.29%	0.43%	0.68%	2631	B2020+McSw	4.36	R2008	862	441	57	1.2	0.14

Table 5

Click here to download Table: Table 5-oxygen isotopes summary with17O.xlsx

meteorite	d18O	d17O	D17O	n	Ref
CV3 OxA					
Allende	1.71	-2.56	-3.45	4	C&M1999, G2010, this study
Axtell	1.52	-2.56	-3.35	2	C&M1999, G2010, this study
ALH 84028	0.54	-3.71	-3.99	3	C&M1999, G2010, this study
ALH 81003	1.80	-3.09	-4.03	3	G2010, this study
GRA 06101	0.84	-3.69	-4.13	1	this study
LAP 02206	4.01	-0.59	-2.68	1	this study
NWA 11589	-1.20	-5.36	-4.73	1	this study
CV3 OxB					
Bali	3.40	-1.13	-2.89	2	C&M1999, G2010
ALH 85006	0.17	-3.82	-3.91	1	G2010
Grosnaja	3.08	-1.62	-3.22	1	G2010
Kaba	1.87	-2.50	-3.47	1	G2010
LAR 06317	0.01	-3.74	-3.75	2	this study
Mokoia	3.04	-1.38	-2.96	2	C&M1999, G2010
MCY 05219	2.66	-2.31	-3.70	1	this study
MET 00761	2.16	-2.45	-3.57	1	this study
NWA 11533	3.83	-1.07	-3.06	1	this study
NWA 11546	1.66	-2.52	-3.38	1	this study
CV3 Ox					
FRO 97002	2.45	-2.16	-3.43		MDB
NWA 6746	0.84	-3.90	-4.34		MDB
NWA 7110	3.94	-1.01	-3.06		MDB
Khawr al Fazra 005	1.77	-2.89	-3.81		MDB
CV3 Red					
Arch	0.08	-4.42	-4.46	2	C&M1999, G2010
Bukhara	0.00	-4.87	-4.87	2	this study
Efremovka	-1.83	-5.51	-4.55	2	C&M1999, G2010
GRO95652	-3.42	-6.91	-5.13	1	G2010
Leoville	-2.44	-6.55	-5.28	2	C&M1999, G2010
MIL 07277	0.72	-3.94	-4.31	1	this study
NWA 8331	-0.78	-4.60	-4.20	4	MDB
NWA 12523	-0.33	-4.60	-4.43	1	this study
QUE 93429	-3.32	-7.00	-5.27	1	C&M1999
QUE 97186	1.71	-2.74	-3.63	1	this study
RBT0 4143	-0.42	-4.30	-4.08	1	this study
RBT0 4302	-0.51	-4.30	-4.03	1	this study
DaG 1063	-0.48	-4.32	-4.07	1	MDB
NWA 2044	-1.92	-5.41	-4.41	2	MDB

Table 4

Click here to download Table: Table 4-oxygen isotopes CEREGE with17O.xlsx

meteorite	d18O □	d17O □	D17O □	initial sample mass (mg)	n
CVOxA					
Allende	1.828	-2.650	-3.601	84	1
ALH 84028	3.022	-1.623	-3.194	9	1
GRA 06101	0.841	-3.692	-4.129	52	1
LAP 02206	4.013	-0.590	-2.677	46	1
NWA11589	1.550	-2.748	-3.554	250	1
CVOxB					
LAR 06317	0.010	-3.743	-3.748	50	2
MCY 05219	2.661	-2.312	-3.696	36	1
MET 00761	2.155	-2.445	-3.566	25	1
NWA 11533	3.830	-1.065	-3.057	161	1
NWA 11546	1.658	-2.522	-3.384	604	1
CVRed					
Bukhara	-0.004	-4.872	-4.870	10	2
MIL 07277	0.720	-3.937	-4.311	69	1
NWA 8331	-0.775	-4.600	-4.197	205	4
NWA 12523	-0.326	-4.595	-4.425	256	1
QUE 97186	1.707	-2.741	-3.629	18	1
RBT 04143	-0.421	-4.295	-4.076	20	1
RBT 04302	-0.509	-4.298	-4.033	13	1

Table 3

Click here to download Table: Table 3-Ks Test.xlsx

CVOx versus CVRed	n CVOx	n CVRed	p
matrix abundance	32	19	1.23E-04
δ18O	21	16	6.00E-05
chondrule diameter	1792	1015	6.78E-10

CVOxA versus CVOxB	n CVOxA	n CVOxB	p
matrix abundance	14	18	2.95E-01
δ18O	7	10	1.17E-01
chondrule diameter	706	1086	5.60E-02

Table 2

Click here to download Table: Table 2-CV average properties.pdf

	matrix abundance			Ni content in sulfides			Metal abundance			Magnetic susceptibility			Chondrule apparent diameter			Chondrule aspect ratio	
	vol%	sd	n	wt%	s.d.	n	vol%	sd	n	logX	sd	n	µm	s.d.	n	average	s.d.
CVOxA	51,3%	7,4%	14	9,55	4,31	14	0,43	0,41	14	3,60	0,26	15	796	426	705	1,225	0,062
CVOxB	53,2%	6,7%	18	18,04	3,96	18	0,09	0,11	11	4,38	0,23	18	749	427	1086	1,296	0,073
CVOx	52,3%	7,0%	32	14,32	5,89	32	0,28	0,36	25	4,03	0,46	33	768	428	1791	1,265	0,062
CVRed	40,3%	7,1%	19	0,34	0,61	19	1,64	1,32	18	4,27	0,39	19	860	477	1015	1,332	0,066

Figure S1

Click here to download Supplementary material for online publication only: Figure S1-elipsoids flattening.pdf